Master of Science

EFFECT OF FRICTION
ON AFM-BASED INDENTATION

The Graduate School
of the University of Ulsan
Department of Mechanical Engineering
Le Tuan Em

EFFECT OF FRICTION

ON AFM-BASED INDENTATION

Supervisor: Professor Koo-Hyun Chung

A Thesis

Submitted to
the Graduate School of the University of Ulsan
In partial Fulfillment of the Requirements
for the Degree of

Master of Science in Mechanical Engineering

by

Le Tuan Em

Department of Mechanical Engineering

University of Ulsan, Korea

November 2019

EFFECT OF FRICTION

ON AFM-BASED INDENTATION

This certifies that the master's thesis

of Le Tuan Em is approved.

Committee Chair Prof. Doo-Man Chun

Committee Member Prof. Dong-Kyu Kim

Committee Member Prof. Koo-Hyun Chung

Department of Mechanical Engineering

University of Ulsan, Korea

November 2019

TABLE OF CONTENTS

LIST OF TABLES

LIST OF FIGURES

ABSTRACT

Atomic force microscopy (AFM)-based indentation measurements have been increasingly used for mapping mechanical properties of materials at the nano-scale. Indentation of an interesting specimen can be obtained as a function of applied force from AFM-based indentation measurements. By interpret force-indentation curves using appropriate contact models, mechanical properties such as elastic modulus of the specimen can be determined.

In a conventional AFM, cantilever deflection is assumed to be a result of normal forces (e.g., adhesion forces, elastic force from specimen), and response of a specimen is assumed to be perfectly elastic for the uses of contact models. However, several factors influence results of AFM-based indentation such as viscoelastic behavior of specimens, creep and hysteresis of piezo-actuator which was used to drive the AFM cantilever, and sliding of an AFM tip against a specimen. In certain cases, effect of viscoelastic behavior and hysteresis of piezo-actuator on force-indentation curves can be reduced whereas effect of friction may not be avoidable. Friction arising from sliding may generate an additional torque to the normal bending moment acting on the AFM cantilever. The frictional torque enhances and reduces the cantilever deflection in extension and retraction during AFM-based indentation measurements, respectively, and thereby generate a difference between elastic moduli determined from extension and retraction curves. Considers cantilever deflection under normal and friction forces during AFM-based indentation, friction-induced hysteresis in force-indentation curves as difference between extension and retraction curves can be partly compensated. Furthermore, the difference between extension and retraction curves due to friction can be examined to give information about friction between tip and specimen.

In this work, effect of friction on force-indentation curves obtained from an AFM was theoretically and experimentally investigated. A theoretical model based on the cantilever

behavior and contact mechanics analysis was proposed for compensating effect of friction in determination of elastic moduli from force-indentation curves, and in turn obtain friction properties between tip and specimen from the difference between extension and retraction curves. Three polymers such as low-density polyethylene, polyethylene naphthalate, and polymethyl methacrylate were used as specimens. Elastic modulus and friction coefficients determined from force-indentation curves obtained on the specimens were validated by the literature and results from lateral force measurements, respectively. In addition, AFM probes with colloidal tips that were different in radius were used. Contribution of relative size of AFM colloidal tip radius to AFM cantilever length on friction-induced hysteresis in force-indentation curves was also investigated. This work was expected to improve the accuracy of elastic properties measurements using an AFM. Furthermore, the proposed model was expected to be particularly helpful for investigation of in-situ relationship between friction properties and deformation in elastic contact from fundamental tribological point of view.

1. INTRODUCTION

1.1 Background and motivation

Measurement of mechanical properties at the nano-scale is one of the great challenges of material characterization. AFM-based indentation measurements were shown to be a suitable candidate for mapping mechanical properties of materials at the nanoscales [1-3]. The principal components of an AFM are a micro-cantilever bearing a tip at its end, and a piezo-actuator that is used to drive the cantilever in a vertical direction. An interesting specimen can be placed under the AFM tip such that distance between the tip and specimen can be controlled by extension or retraction of the piezo-actuator. Interaction forces between the tip and specimen can be revealed from cantilever deflection during the extension and retraction motion. Difference between piezo-actuator displacement and cantilever deflection during the interaction between the AFM tip and the specimen can be referred to as specimen indentation. Force-indentation curves can be interpreted using a proper contact model to determine mechanical properties such as elastic modulus of the interesting specimen.

Several factors may influence results from AFM-based indentation. For example, viscoelastic behavior of a specimen may induce hysteresis between extension and retraction portions of force-indentation curves. It was suggested that speed of indentation should be in a time range that larger than the relaxation time of the specimens to reduce the effect of the viscoelastic behavior [1]. In addition, creep and hysteresis of piezo-actuator may also be concerned. Hysteresis of the piezo-actuator can be eliminated by the uses of a closed-loop control system [4]. In a conventional AFM, the AFM cantilever is usually mounted at a tilt angle with an intention to secure that only the AFM tip interacts with an interesting specimen during AFM-based indentation measurements [5]. The tilt angle of the cantilever causes

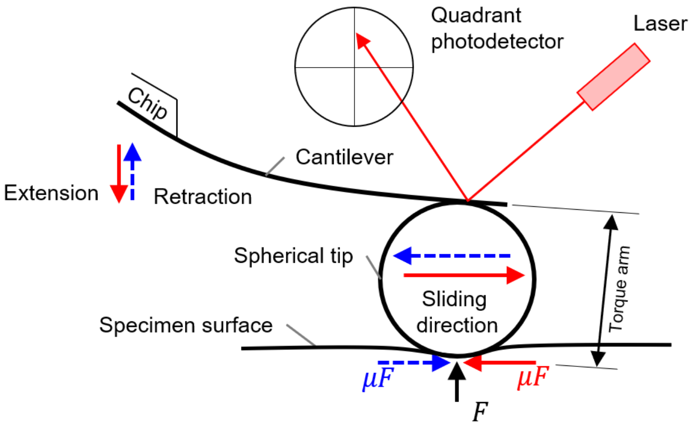

Figure 1.1 An illustration of effect of friction on AFM-based indentation

sliding of the AFM tip against a specimen, and this gives rise to a tangential force attributed to the friction characteristics between the AFM colloidal tip and specimen, as shown in Figure 1.1. In consequence, the friction force generates an additional torque to the normal bending moment acting on the cantilever, and in turn leads to underestimation and overestimation of cantilever deflection according to extension and retraction motion of the piezo-actuator, respectively [6-11]. Recent studies indicate that friction-induced hysteresis in force-indentation curves may further contribute to underestimation or overestimation of elastic moduli obtained from extension or retraction curves [12,13]. It was found that the underestimation or overestimation of elastic moduli due to friction can be compensated. Furthermore, examination of the difference between extension and retraction portions of force-indentation curves can give information of friction properties between a tip and specimen.

1.2 Objectives of the thesis

The objective of this work is to compensate for effect of friction on determination of elastic properties from force-indentation curves obtained from an AFM, and in-turn assess friction properties from difference between extension and retraction curves. To do so, a theoretical model based on cantilever behaviors and contact mechanics analysis for in-situ determination of elastic and frictional properties from AFM-based indentation data. To do so, a theoretical model was developed based on the cantilever behavior and contact mechanics analysis. Force-indentation curves were obtained on three different polymeric specimens of low-density polyethylene (LDPE), polyethylene naphthalate (PEN) and polymethyl methacrylate (PMMA). Elastic and frictional properties of the specimens were obtained using the proposed model, and in turn validate by those taken from the literature and results of lateral force measurements, respectively. Furthermore, contribution of relative size of colloidal tip to cantilever length on friction-induced hysteresis was discussed. The findings from this work were expected to improve accuracy of mechanical property measurements using an AFM, and particularly helpful for investigation of in-situ relationship between friction properties and deformation in elastic contact from fundamental tribological point of view.

1.3 Organization of the thesis

The overall structure of this thesis taken the form of five sections, where the motivation and the objectives of this work have been explained so far in section 1. Section 2 will quantify the cantilever deflection under normal and friction forces, and thereby provides an expression for the determination of normal force from cantilever deflection that considers effect of friction. Specimen deformation because of normal force was addressed by the Johnson-Kendall-Robert model due to lacking an adhesive model that consider friction. Compensation for effect of friction in determination of elastic modulus and determination of friction coefficient from the difference between extension and retraction curves were provided.

In section 3, preparations of AFM colloidal probes and specimens were described. AFM-based indentation measurements and experimental conditions to obtained force-indentation curves on the specimens were represented. To validate friction coefficient determined from force-indentation curves using the proposed model, friction loops were obtained on the specimens using lateral force measurements. Lateral force measurements and experimental conditions were also provided in section 3. For quantitative assessments of elastic and frictional properties, normal and lateral calibrations were provided in detail.

In section 4, elastic moduli that was compensated for effect of friction, and friction coefficients obtained from force-indentation curves using the proposed model were presented. Elastic moduli of specimens determined from force-indentation curves using the proposed model were compared to those taken from the literature. Friction coefficients were compared to those obtained from friction loops. In addition, effect of AFM colloidal tip size on force-indentation curves was discussed. Limitations of this work were also reviewed in this section.

Section 5 concludes the finding of this work. By recognizing the limitations, a few recommendations were discussed for further investigation.

2. THEORETICAL MODELING

Illustration of an AFM colloidal tip pressing into an elastic specimen and cantilever deflection under normal and friction forces, F_{n} and F_{f}, in AFM-based indentation measurements was shown in Figure 2.1(a) . The colloidal tip is assumed to be rigid, and the specimen surface was assumed to be parallel to the horizontal direction when it is undeformed. Deformation of specimen generates a normal force acting on the colloidal tip. Also, a friction force arises from sliding between the colloidal tip and the specimen. The friction force was assumed to be proportional to the normal force by a friction coefficient μ such that friction force can be expressed as $F_{\mathrm{f}} = \mu F_{\mathrm{n}}$. To quantify torques acting on the cantilever, the normal and friction forces were decomposed into force components those are parallel and perpendicular to the cantilever longitudinal axis, as shown in Figure 2.1(b).

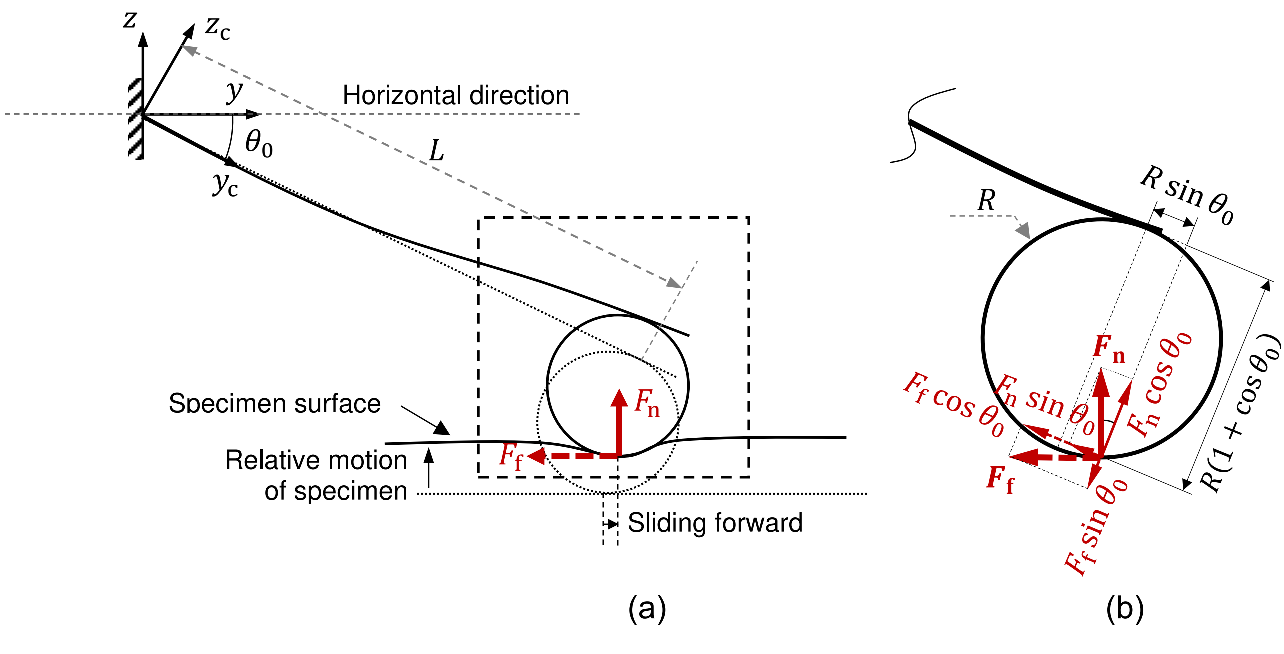

Figure 2.1 (a) An illustration of an AFM probe with colloidal tip pressing into an elastic specimen and (b) force components acting on the colloidal tip.

Mathematical description of torques acting on the cantilever can be expressed as a matrix multiplication of lever arms and decomposition of normal and friction forces, as shown in Eq. (1).

$$-E_c I \frac{\partial^2 z_c}{\partial y_c^2} = \begin{bmatrix} R(1+\cos\theta_0) & L + R\sin\theta_0 - y_c \end{bmatrix} \begin{bmatrix} -\sin\theta_0 & \cos\theta_0 \\ \cos\theta_0 & \sin\theta_0 \end{bmatrix} \begin{bmatrix} F_n \\ \mp F_f \end{bmatrix} \quad (1)$$

where E_c and I are elastic modulus and area moment of inertia of the cantilever, respectively. The minus and plus signs indicate that the direction of the friction force is in opposition to the sliding forward and backward during extension and retraction motion of piezo-actuator, respectively. θ_0 is tilt angle of the AFM cantilever, L and R indicate cantilever length (i.e., distance from the fix end of cantilever to the point where the colloidal tip is attached) and radius of the AFM colloidal tip radius, respectively.

Cantilever deflection in the direction to the specimen surface, Δz, obtained from the torque given in Eq. (1) was shown in Eq. (2).

$$\Delta z = \frac{F_n}{k_c}(\eta_n \mp \mu\eta_f) \quad (2)$$

where $\eta_n = \left(\cos^2\theta_0 - \frac{3R}{2L}\sin\theta_0\cos\theta_0\right)$ and $\eta_f = \cos\theta_0\left[\sin\theta_0 + \frac{3R}{2L}(1+\cos\theta_0)\right]$. Values of $(\eta_n \mp \mu\eta_f)$ represents the variation of cantilever deflection due to the tilt angle, relative size of AFM colloidal tip to cantilever length (i.e., R/L ratio), and friction between the AFM colloidal tip and the specimen. The subscript of minus and plus signs on η indicates the value is used for extension and retraction data, respectively. $k_c = 3E_c I/L^3$ is the intrinsic cantilever stiffness.

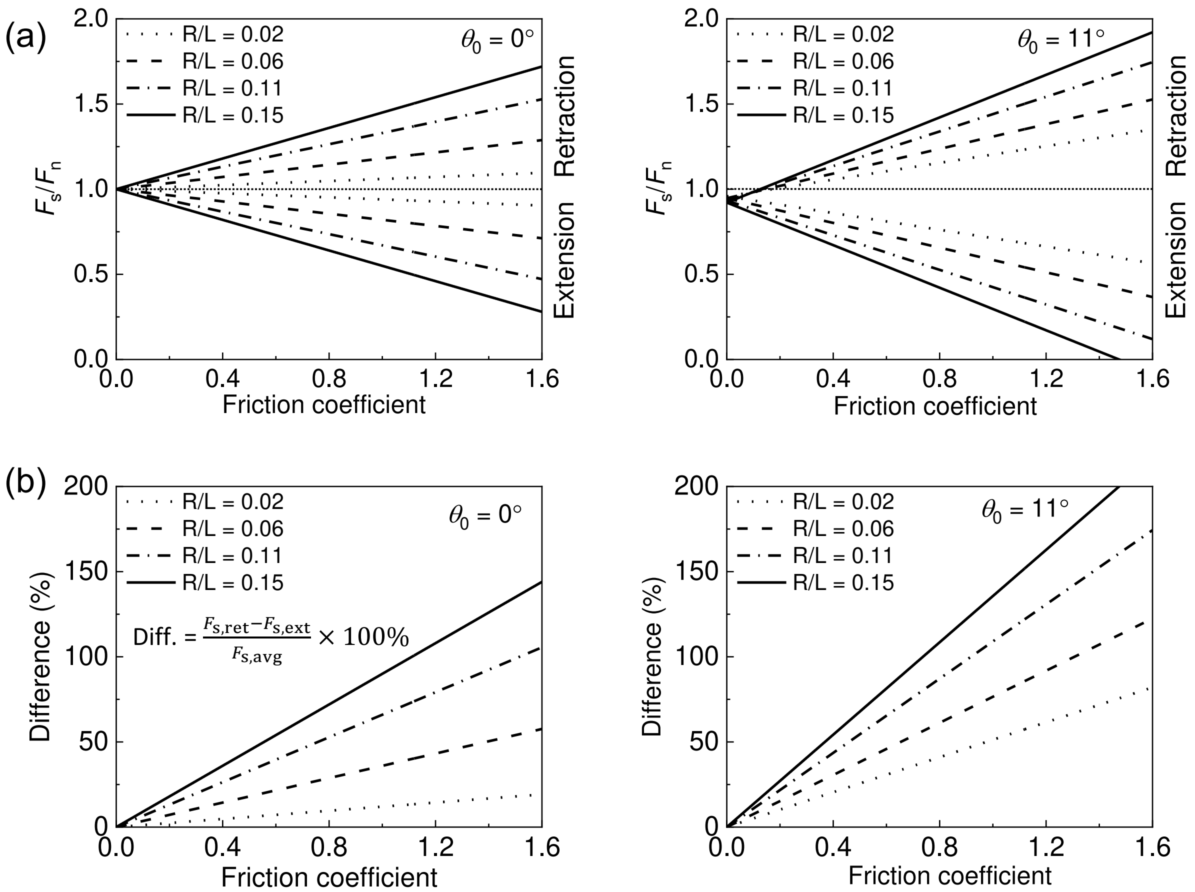

Figure 2.2 (a) Underestimation and overestimation of, and (b) difference between normal forces detected from the optical lever scheme during extension and retraction motions

In the conventional method of analyzing force data from an AFM, determination of normal force from cantilever deflection, that was converted from optical lever voltage ΔV involving normal optical lever sensitivity s_{N}, simply requires knowledge of the cantilever stiffness, i.e., $F_{\mathrm{s}} = k_{\mathrm{c}}\Delta z = k_{\mathrm{c}} s_{\mathrm{N}} \Delta V$. The subscript of ‘s’ on F indicate force directly detected from cantilever deflection obtained from optical lever scheme of an AFM. Calibration of s_{N} may be influenced by the tilt angle, AFM tip shape and size, and friction between the AFM tip and substrate [6-11], This further contributes to uncertainty in determination of k_{c} in a few calibration methods [14]. Also, F_{s} could be different with the “actual” normal force F_{n} due to friction. The difference between F_{s} and F_{n} can be revealed by examining the ratio of

$F_s/F_n = (\eta_n \mp \mu\eta_f)$, as shown in Figure 2.2. The examination considers two case of cantilever mounting such as horizontal and tilted an angle of 11°. Also, four values of R/L ratio ranged from 0.02 to 0.15 were also considered.

In general, Figure 2.2(a) shows that the higher friction leads to the larger deviation of F_s/F_n value from 1.0. This suggests that friction leads to a deviation of F_s from F_n. For the case of horizontal cantilever, values of F_s determined in extension and retraction data, $F_{s,ext}$ and $F_{s,ret}$, tends to be underestimated and overestimated, respectively, due to friction. If assuming friction coefficient is equal between sliding direction of the tip forward and backward against the specimen, difference between $F_{s,ext}$ and $F_{s,ret}$ is almost certainly symmetric. Also, the difference tends to be more significant for larger friction, as shown in Figure 2.2(b). In practical, AFM cantilevers are usually mounted at a tilt angle, typically 11°, for securing that only the tip touches the specimen [5]. In Figure 2.2(b), $F_{s,ext}$ and $F_{s,ret}$ are also underestimated and overestimated, respectively. Difference between $F_{s,ext}$ and $F_{s,ret}$ due to friction for the case of tilt cantilever was shown to be more significant comparing to the horizontal one. Tilt angle and R/L ratio also lead to systematical underestimation of both $F_{s,ext}$ and $F_{s,ret}$. Correction factors for such underestimation were proposed in the literature [14,15].

Assuming effect of friction is symmetric, effect of the tilt angle, R/L ratio and friction on F_s can be compensated for determination of F_n as Eq. (3).

$$F_n = F_s/(\eta_n \mp \mu\eta_f) \tag{3}$$

Friction may influence contact geometry between a tip and a specimen. Assuming a non-adhesive contact between AFM tips and specimens used in this work, deformation profiles of specimens with experimental conditions given in section 3 were shown in Figure 2.3(a)

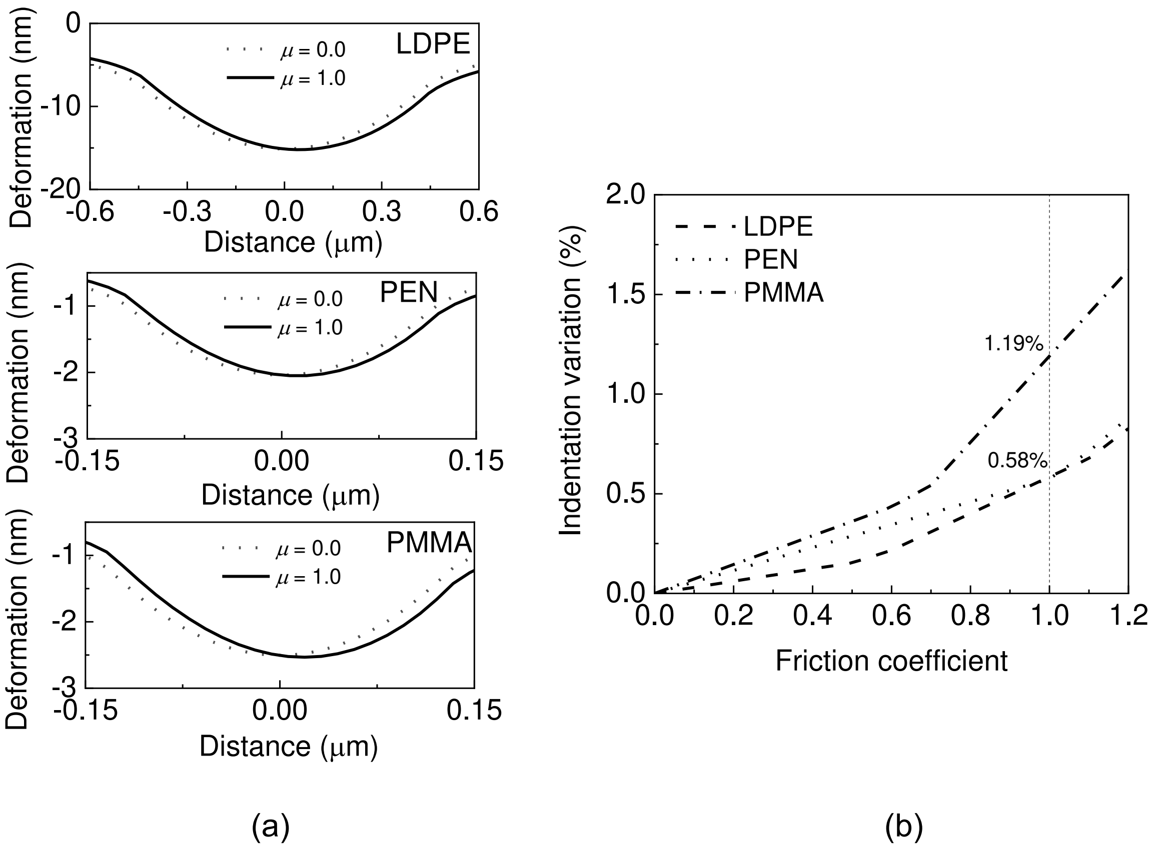

Figure 2.3 Deformation profiles of LDPE, PEN and PMMA specimens under normal and friction forces with μ = 1, and, (b) indentation variation according to increasing friction.

[16]. It can be seen from Figure 2.3(a) that deformation of the specimen slightly changes under a combination of normal and friction forces compared to that under a pure normal force. By assuming that indentation is the maximum deformation, indentation variation corresponding to friction coefficient ranged from 0.0 to 1.2 was shown in Figure 2.3(b). It can be seen that the indentation increases around 1.19% when friction coefficient reaches 1.0. The indentation variation was shown to be likely small in the presence of friction. In particular, the specimens used in this work have relatively large adhesion, an adhesive contact model that consider friction should be used. Contact area of an adhesive contact was experimentally observed to be slightly reduced in the presence of friction [17]. However, a theoretical contact model that consider sliding friction is likely not available in the literature.

Accepting that limitation, the JKR model was used to describe the relationship between normal force and indentation of specimens used in this work.

Relationship between indentation and normal force based on JKR model can be given as Eq. (4) [18,19].

$$\delta = \frac{a_0^2}{R}\left[\left(\frac{1+\sqrt{1+F_\mathrm{n}/F_\mathrm{ad}}}{2}\right)^{4/3} - \frac{2}{3}\left(\frac{1+\sqrt{1+F_\mathrm{n}/F_\mathrm{ad}}}{2}\right)^{1/3}\right] \quad (4)$$

$$a_0 = \left[\frac{9\pi R^2\gamma}{2}\left(\frac{1-\nu_\mathrm{t}^2}{E_\mathrm{t}} + \frac{1-\nu_\mathrm{s}^2}{E_\mathrm{s}}\right)\right]^{1/3} \quad (5)$$

where δ is indentation of specimen and can be determined as difference between piezo-actuator displacement and cantilever deflection. Adhesion force F_ad can be a function of work of adhesion γ as $F_\mathrm{ad} = \frac{3}{2}\pi R\gamma$. Contact area under a zero normal force, a_0, can be determined as Eq. (5) where E_t and E_s, are elastic moduli, ν_t and ν_s, are Poisson's ratio of the tip and specimen, respectively.

The relationship given in Eq. (4) was modified to correct effect of friction on the normal force detected from the optical lever sensitivity, as shown in Eq. (6).

$$\delta = \alpha\left[\left(\frac{1+\sqrt{1+F_\mathrm{s}/\beta}}{2}\right)^{4/3} - \frac{2}{3}\left(\frac{1+\sqrt{1+F_\mathrm{s}/\beta}}{2}\right)^{1/3}\right] \quad (6)$$

where constants $\alpha = a_0^2/R$ and $\beta = (\eta_\mathrm{n} \mp \mu\eta_\mathrm{f})F_\mathrm{ad}$ can be determined from curve fitting.

The difference between extension and retraction curves can be revealed through the difference between values of α and β determined from fitting of extension and retraction data, α_ext and α_ret, and, β_ext and β_ret, respectively. Subscripts 'ext' and 'ret' on α and β denote the values determined from fitting of extension and retraction curves, respectively.

Elastic modulus can be determined from α and β determined from extension or retraction curves, using Eq. (7).

$$E_{\mathrm{s}} = (1-\nu_{\mathrm{s}}^{2})\left[\frac{(\eta_{\mathrm{n}}-\mu\eta_{\mathrm{f}})\sqrt{R}\alpha_{\mathrm{ext}}^{\frac{3}{2}}}{3\beta_{\mathrm{ext}}}-\frac{1-\nu_{\mathrm{t}}^{2}}{E_{\mathrm{t}}}\right]^{-1}$$

or (7)

$$E_{\mathrm{s}} = (1-\nu_{\mathrm{s}}^{2})\left[\frac{(\eta_{\mathrm{n}}+\mu\eta_{\mathrm{f}})\sqrt{R}\alpha_{\mathrm{ret}}^{\frac{3}{2}}}{3\beta_{\mathrm{ret}}}-\frac{1-\nu_{\mathrm{t}}^{2}}{E_{\mathrm{t}}}\right]^{-1}$$

However, friction coefficient is needed to be known for compensating the friction-induced hysteresis in determination of E_{s} from curve fitting. Determination of friction coefficient requires other methods such as lateral force measurements, and it may not reveal exactly local friction properties between tip and specimen during AFM-based indentation measurements. On the other hand, assuming isotropic friction between extension and retraction, the difference between extension and retraction curves can be examined to yield friction properties between tip and specimen. Friction lead to underestimation and overestimation of normal force, and hence, elastic moduli obtained from extension and retraction curves are underestimated and overestimated, respectively. Assuming no plastic deformation in either extension and retraction, elastic moduli obtained from extension and retraction curves should be identical. By equating elastic moduli determined from extension and retraction curves using Eq. (7), friction coefficient can be determined from the ratio of α and β fitted from extension and retraction curves. In particular, since this approach was based on the JKR model, applying fitting on both extension and retraction curves may leads to hysteresis of work of adhesion determined from extension and retraction data [20]. Discussion of hysteresis of work of adhesion was out-of-scope of this work. Friction coefficient can be determined from the difference between extension and retraction curves using Eq. (8).

$$\mu = \frac{\eta_{\mathrm{n}}\left(\alpha_{\mathrm{ext}}^{3/2}\beta_{\mathrm{ret}} - \alpha_{\mathrm{ret}}^{3/2}\beta_{\mathrm{ext}}\right)}{\eta_{\mathrm{f}}\left(\alpha_{\mathrm{ext}}^{3/2}\beta_{\mathrm{ret}} + \alpha_{\mathrm{ret}}^{3/2}\beta_{\mathrm{ext}}\right)} \tag{8}$$

Value of friction coefficient determined from Eq. (8) can be used to compensate for the friction-induced hysteresis in determination of elastic modulus using Eq. (7). Finally, friction coefficient and elastic modulus can be determined from force-indentation curves.

3. EXPERIMENTAL DETAILS

Polymers often have relatively large friction [13], and therefore chosen as specimens to clearly observe the effect of friction on force-indentation curves. Three specimens such as LDPE, PEN, and PMMA with different elastic and frictional properties were selected to generalize the proposed model. LDPE, PEN, and PMMA films were purchased from manufactures with thickness of 15 μm, 12 μm, and 130 μm, respectively. Since LDPE specimen is soft and flexible, it was clamped on a relatively large curvature steel substrate to avoid unexpected membrane deformations. PEN and PMMA specimens were glued to bare Si substrates using epoxy. Thickness of the specimens is relatively large, and hence, effect of different substrates on the specimens likely to be not significant. Investigation of effect of different substrates on force-indentation curves was out-of-scope of this work. AFM topography images of the specimens were observed using a Si probe (AC240, Olympus) by intermittent contact mode, as shown in Figure 3.1. Average surface roughness

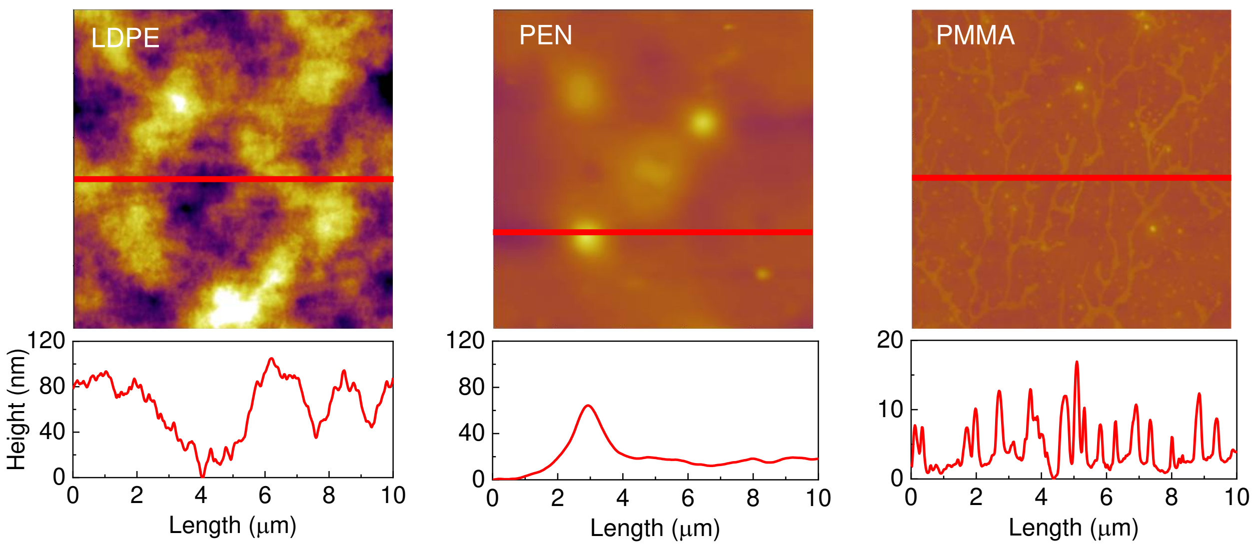

Figure 3.1 Topography images of the LDPE, PEN and PMMA specimens.

values of the LDPE, PEN, and PMMA specimens were determined to be approximately 21.9 ± 1.8 nm, 6.2 ± 1.3 nm, and 2.4 ± 0.1 nm, respectively (mean ± 1 standard deviation), via AFM topographic images obtained at eight difference scanning area of 10 μm × 10 μm. Poisson's ratio of LDPE, PEN, and PMMA specimens were taken from literature (0.40, [21], 0.40 [2], and 0.35 [22], respectively) for the determination of elastic moduli of specimens from force-indentation curves using contact models.

Two AFM probes with different colloidal tips were chosen to obtain force-indentation curves within elastic region. Each AFM probe were made by attaching an Au colloidal

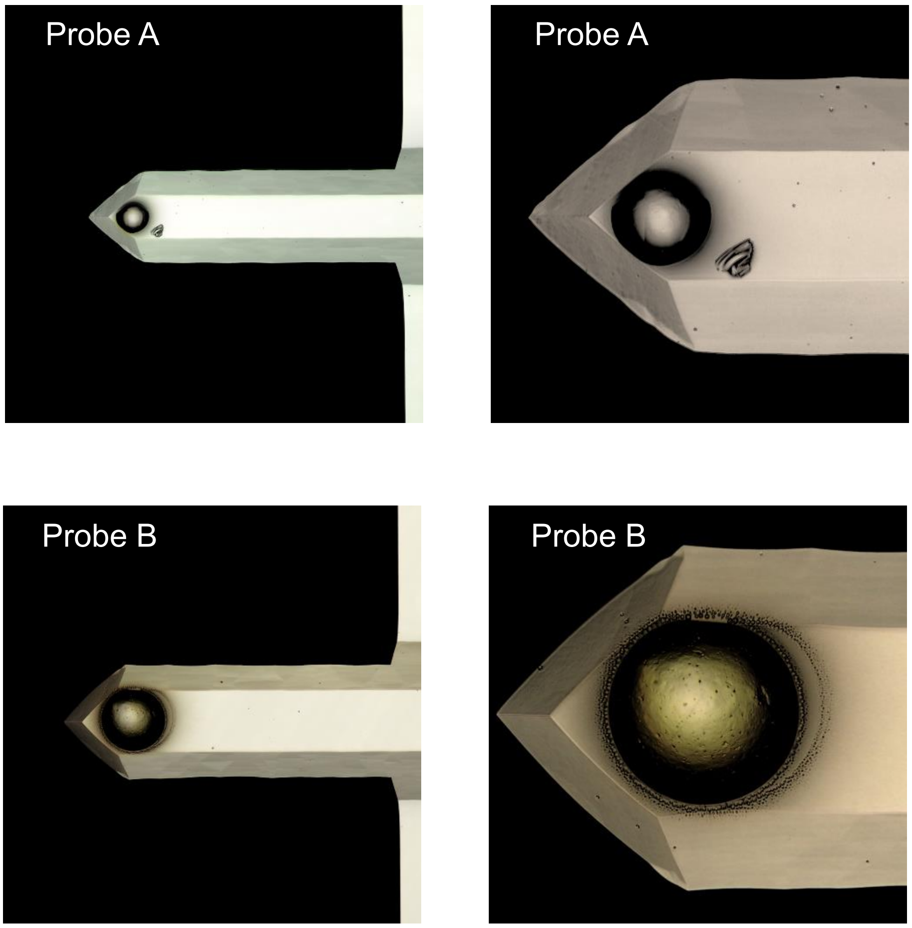

(a) (b)

Figure 3.2 Confocal microscopy images of AFM probes A and B.

particle on the underside of a tipless cantilever (TL-NCH, Nanosensors). The tipless cantilevers with nominal spring constant of 42 N/m was chosen to apply appropriate forces so that indentation could be measurable during AFM-based indentation measurements [22]. Dimensions of the AFM probes were determined using confocal microscopy (VK-X200, Keyence), as shown in Figure 3.2. Tip radii of the two probes, A and B, were measured to be 6.3 μm and 12.7 μm, respectively. AFM cantilevers of probes A and B were assumed to be rectangular with average width, thickness, length, were measured to be 28.8 μm and 37.3 μm, 4.1 μm and 3.9 μm, and, 113.5 μm and 112.3 μm, respectively. The elastic modulus and Poisson's ratio of Au was taken from literature (78 GPa and 0.42, respectively) for the interpretation of force-indentation curves using contact models [23]. Also, the elastic modulus of Si was taken from literature (169 GPa and 0.3, respectively) for determination of lateral spring constant for the lateral force measurements [24].

A commercial AFM (MFP-3D, Asylum research) was used to obtain force-displacement curves. The AFM probes were carefully mounted such that lateral deflection during AFM-based indentation measurements could be minimized. Cantilever deflection was determined

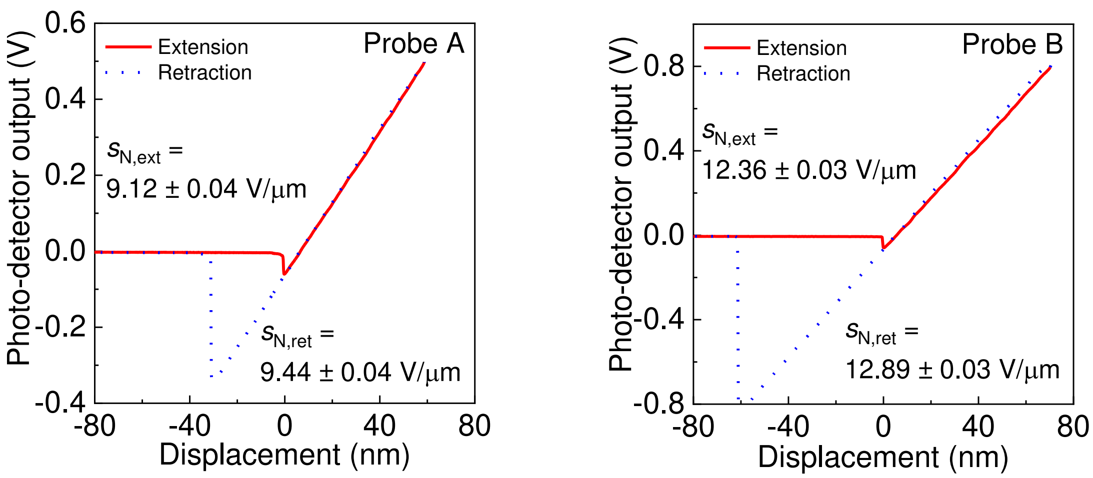

Figure 3.3 Photo-detector output versus piezo-actuator displacements obtained on bare Si substrate using AFM probe A and B.

from photo-detector output and normal optical lever sensitivity s_{N}. Indentation of specimen was determined as difference between displacement of piezo-actuator and cantilever deflection. s_{N} was determined from compliance slopes of photo-detector output in voltages versus the piezo-actuator displacement in nanometers obtained on a bare Si substrate, as shown in Figure 3.3. s_{N} obtained from retraction curves were consistently larger than that obtained from extension curves on the scale of 3.5% and 4.3% for the probes A and B, respectively, those may due to friction [6-8,10,11,25]. s_{N} values of the probes A and B were determined to be 9.3 ± 0.2 V/μm and 12.6 ± 0.3 μm, respectively.

Cantilever spring constant, k_{c}, of the AFM probes was determined using thermal noise method [26]. Effect of cantilever tilt on determination of k_{c} is likely small [14], and it was neglected in this work. k_{c} values of probe A and B were obtained to be 50.2 ± 0.5 N/m and 38.0 ± 0.1 N/m, respectively, based on three measurements. Force-indentation curves were obtained at maximum normal force to be 2.0 μN to secure observable indentation of specimens. The speed of AFM-based indentation measurements was maintained to be quiet slow of 100 nm/s to minimize the effect of viscoelastic behavior [1]. Investigation on viscoelastic behavior of the specimens were beyond the scope of this work.

200 force-indentation curves were obtained on random locations of each specimen. Elastic moduli of the specimens were obtained from extension and retraction curves of the force-indentation curves using the JKR model included in the Asylum Research (AR version 14.20.152). In addition, force-indentation curves were interpreted by Eq. (6) using MATLAB (The MathWorks, Inc., Natick, Massachusetts, United States). Hence, elastic moduli of specimens and friction coefficients between the colloidal tip and the specimens were determined using Eqs. (7-8).

In order to cross-check the friction coefficients obtained from force-indentation curves using the proposed model, the friction loops were obtained using lateral force measurements. The friction loops were obtained at five different normal forces such as ranged from 0.2 μN to 1.0 μN. 160 friction loops obtained on different locations at each normal force. Lateral force calibration was performed after the lateral force measurements to minimize tip wear during calibration. More than ten friction loops were obtained at different normal forces (i.e., 0.2 μN and 0.5 μN) on a bare Si substrate, and hence, the lateral optical deflection sensitivity, s_{L}, was determined from slopes of the friction loops when the colloidal tip stick to the substrate [27]. s_{L} values of probes A and B were obtained to be 8.8 ± 1.3 V/μm and 14.4 ± 0.3 V/μm, respectively. Cantilevers of probes A and B were assumed to be rectangular, and lateral spring constants were determined to be 1091.6 N/m and 535.9 N/m, respectively [28,29]. The lateral sensitivities of probe A and B were determined to be 7.9 mV/μN and 26.6 mV/μN, respectively. Friction forces were determined from friction signal from friction loops and the lateral sensitivities. The friction signal was determined to be a half of difference between average lateral signal during forward scan and backward scan in a friction loop. Friction coefficients of specimens were determined as slopes of linear relationship between friction and normal forces.

4. RESULTS AND DISCUSSION

Figure 4.1(a-b) shows force-displacement curves and force-indentation curves for LDPE, PEN, and PMMA specimens. It was observed that extension and retraction portions of force-displacement curves are slightly different to each other. The differences were more obvious in force-indentation curves. The JKR model fit given in Eqs. (4-5) was applied to extension and retraction curves. It can be observed that initial portions of extension curves, and transition from extension to retraction curves, were not well fitted with the JKR model that may due to sticking of the tip to the specimens. Elastic moduli obtained from extension and retraction curves, $E_{\mathrm{s,ext}}$ and $E_{\mathrm{s,ret}}$, respectively, of force-indentation curves shown in Figure 4.1(b) are 0.08 GPa and 0.19 GPa, 1.35 GPa and 11.92 GPa, and, 1.16 GPa and 5.58 GPa, for the LDPE, PEN, and PMMA specimens, respectively. In order to compare the difference between $E_{\mathrm{s,ext}}$ and $E_{\mathrm{s,ret}}$ among specimens, the difference in percent can be determined as $2 \times (E_{\mathrm{s,ret}} - E_{\mathrm{s,ext}})/(E_{\mathrm{s,ret}} + E_{\mathrm{s,ext}}) \times 100$. For the force-indentation curves shown in Figure 4.1(b), the differences were calculated to be 81%, 159% and 131% for the LDPE, PEN, and PMMA specimens, respectively.

As for statistical analysis, $E_{\mathrm{s,ext}}$ and $E_{\mathrm{s,ret}}$ values were obtained from 200 force-indentation curves for each specimen. Histograms of $E_{\mathrm{s,ext}}$ and $E_{\mathrm{s,ret}}$ values, and corresponding mean values $\bar{E}_{\mathrm{s,ext}}$ and $\bar{E}_{\mathrm{s,ret}}$ were shown in Figure 4.1(c). $\bar{E}_{\mathrm{s,ext}}$ and $\bar{E}_{\mathrm{s,ret}}$ values were calculated to be 0.08 ± 0.03 GPa and 0.19 ± 0.06 GPa for the LDPE specimen, 2.19 ± 0.64 GPa and 9.81 ± 3.43 GPa for the PEN specimen, and, 1.86 ± 0.63 GPa and 5.50 ± 1.62 GPa for the PMMA specimen. Relative uncertainties of the $\bar{E}_{\mathrm{s,ext}}$ and $\bar{E}_{\mathrm{s,ret}}$ were calculated to be 38% and 32% for the LDPE specimen, 29% and 35% for the PEN specimen, and, 34% and 29% for the PMMA specimen. Difference between $\bar{E}_{\mathrm{s,ext}}$ and $\bar{E}_{\mathrm{s,ret}}$ values were calculated to be 86%, 123% and 99% for the LDPE, PEN, and PMMA specimens, respectively. Elastic moduli obtained from retraction curves are consistently larger than that obtained from extension curves. As for comparison, elastic moduli of the LDPE, PEN, and PMMA polymers were taken from literature to be 0.19 GPa, 5.25 GPa, and 4.06 ± 0.59 GPa, respectively [2,21]. In general, $\bar{E}_{s,ext}$ values were lower than the referent values whereas the

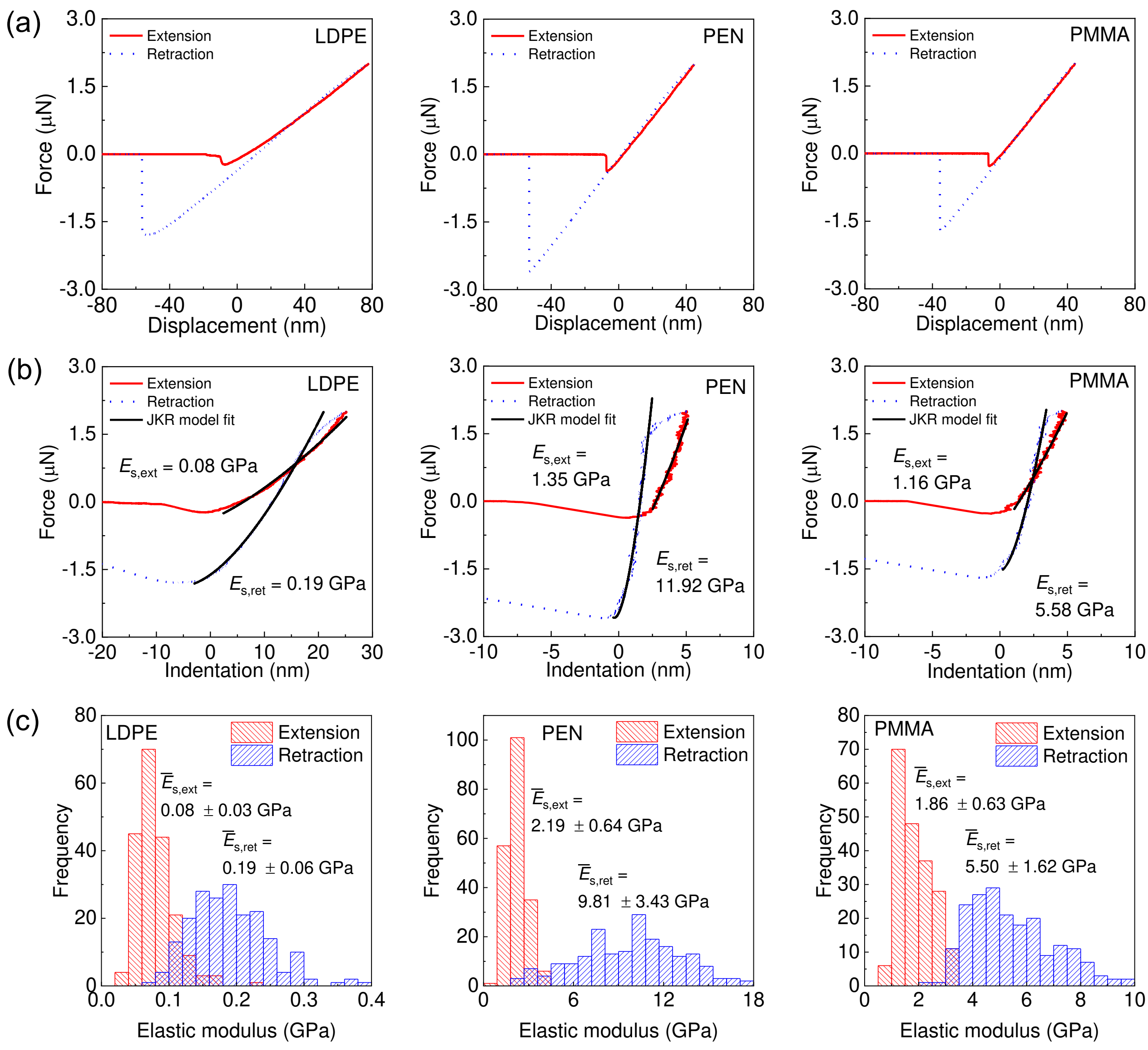

Figure 4.1 (a) Force-displacement curves, (b) force-indentation curves, and, (c) histograms of elastic moduli determined from extension and retraction curves for the LDPE, PEN and PMMA specimens.

$\bar{E}_{\text{s,ret}}$ values were larger than the referent values. It was plausible that the difference between $\bar{E}_{\text{s,ext}}$ and $\bar{E}_{\text{s,ret}}$ values attributes from the effect of friction on force-indentation curves. Elastic moduli after compensated for the effect of friction using the proposed model were shown in Figure 4.2, and corresponding mean values, $\bar{E}_{\text{s}}$, were determined to be 0.14 ± 0.05 GPa, 6.49 ± 2.40 GPa and 4.07 ± 1.20 GPa for the LDPE, PEN and PMMA specimens, respectively. $\bar{E}_{\text{s}}$ of the LDPE specimen was shown to be lower than that taken from the literature. $\bar{E}_{\text{s}}$ of the PEN was shown to be larger than that taken from the literature. The difference may be due to the difference in measurement scale [30]. In general, $\bar{E}_{\text{s}}$ values were shown to fairly agree with elastic moduli of similar polymers taken from the literature [2,21]. By assuming effect of friction on force-indentation curves is symmetric, elastic moduli of the specimen can also be determined as an average value of those obtained from extension and retraction curves, i.e., $E_{\text{s,avg}} = (E_{\text{s,ext}} + E_{\text{s,ret}})/2.0$. Mean values the average elastic moduli, $\bar{E}_{\text{s,avg}}$, were determined to be 0.13 ± 0.04 GPa, 6.00 ± 1.81 GPa and 3.68 ± 0.88 GPa for the LDPE, PEN and PMMA specimens. $\bar{E}_{\text{s,avg}}$ values were observed to be consistently lower than $\bar{E}_{\text{s}}$. This is due to the correction for the tilt angle and R/L ratio was

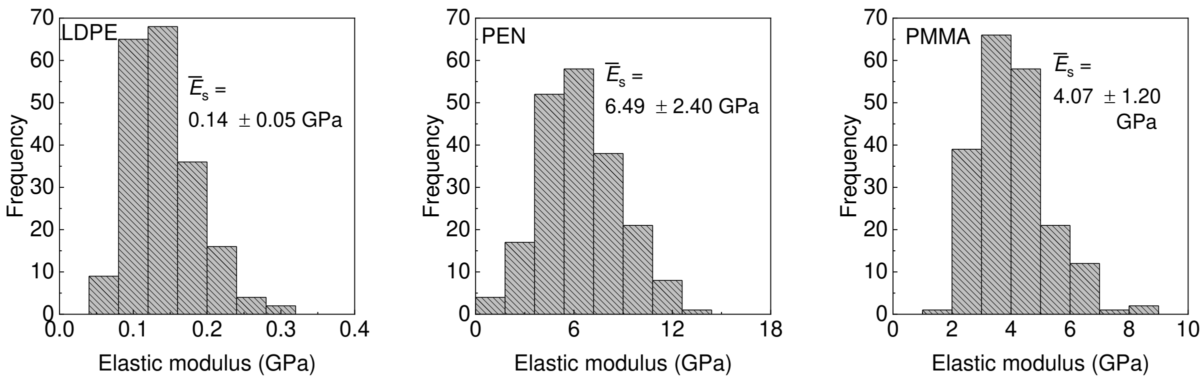

Figure 4.2 Elastic moduli of the LDPE, PEN and PMMA specimens determined using the proposed model.

not considered in determination of $E_{s,ext}$ and $E_{s,ret}$. However, the differences between $\bar{E}_s$ and $\bar{E}_{s,avg}$ values were shown to be not significant. This suggested that $\bar{E}_{s,avg}$ values can be used for roughly estimation of elastic properties of specimens. However, for more accurate measurements, effect of tilt angle and R/L ratio should be considered.

Histograms of friction coefficients of the LDPE, PEN and PMMA specimens obtained from force-indentation curves were shown in Figure 4.3(a). Mean values of friction coefficient, $\bar{\mu}$, were determined to be 0.73 ± 0.32, 1.29 ± 0.45 and 0.87 ± 0.37 for the LDPE, PEN and PMMA specimens, respectively. Relative uncertainties were determined to be 44%,

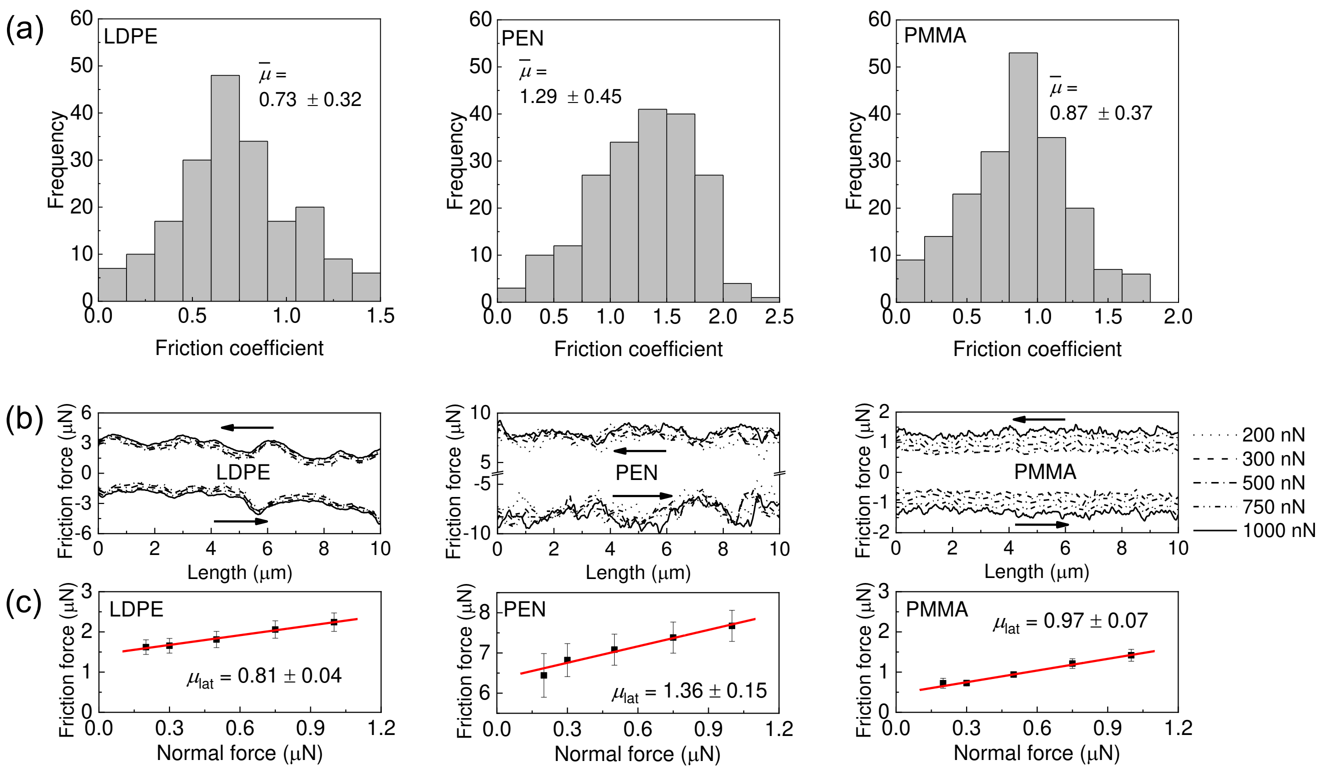

Figure 4.3 (a) Friction coefficient obtained from force-indentation curves using the proposed model, (b) friction loops and (c) relationship between friction and normal forces obtained by the lateral force measurements.

35% and 43%, for the LDPE, PEN and PMMA specimens. It is clearly seen that the higher difference between extension and retraction curves results in the higher friction.

To validate the friction determined from force-indentation curves, friction coefficients were also determined from friction loops. The friction loops obtained on the LDPE, PEN and PMMA specimens were shown in Figure 4.3(b). Relatively large fluctuation in the friction loops may be attributed from surface waviness of the specimens. In particular, large fluctuation observed in friction loops obtained on PEN specimens may be a result of the semi-crystalline structure of the PEN specimen. Friction forces determined from friction loops were shown in Figure 4.3(c). Relationship between friction forces and normal forces were shown to be linear, and friction force is not zero at zero normal force. This may due to large adhesion between tips and specimens. Offset of friction-normal relationship due to adhesion force was not considered in this work. Friction coefficients were determined as slopes of the friction-normal force relationship, μ_{lat}, to be 0.81 ± 0.04, 1.36 ± 0.15 and 0.97 ± 0.07, for the LDPE, PEN and PMMA specimens, respectively. Friction coefficients determined from friction loops were shown to agree with those obtained from force-indentation curves using the proposed model. It was suggested that friction coefficients can be obtained from force-indentation curves.

Elastic and frictional properties of LDPE, PEN, and PMMA specimens obtained in this work were shown in Table 4.1. In general, the difference between $\bar{E}_{\mathrm{s,ext}}$ and $\bar{E}_{\mathrm{s,ret}}$ of the specimens were shown to be as large as 86%. It was suggested that effect of friction on determination of elastic moduli from force-indentation curves obtained on polymers, particularly LDPE, PEN and PMMA, is substantial. In several instances, friction between a tip and specimen should be avoided or minimized for the accuracy in determination of elastic modulus from AFM force-indentation curves.

In particular, polymers often have relatively large friction [13] and consideration of effect of friction in force-indentation curves obtained on polymers using an AFM may be necessary.

Table 4.1 Elastic and frictional properties of LDPE, PEN and PMMA specimens obtained in this work

Specimens	Elastic moduli from extension and retraction curves				Elastic moduli and friction coefficients from force-indentation curves		Results from friction loops	Literature
	$\bar{E}_{s,ext}$ (GPa)	$\bar{E}_{s,ret}$ (GPa)	$\bar{E}_{s,avg}$ (GPa)	Difference (%)[a]	$\bar{E}_s$ (GPa)	$\bar{\mu}$	μ_{lat}	E (GPa)
LDPE	0.08 ± 0.03	0.19 ± 0.06	0.13 ± 0.04	86	0.14 ± 0.05	0.73 ± 0.32	0.81 ± 0.04	0.19 [21]
PEN	2.19 ± 0.64	9.81 ± 3.43	6.00 ± 1.81	123	6.49 ± 2.40	1.29 ± 0.45	1.36 ± 0.15	5.25 [2]
PMMA	1.86 ± 0.63	5.50 ± 1.62	3.68 ± 0.88	99	4.07 ± 1.20	0.87 ± 0.37	0.97 ± 0.07	4.06 ± 0.59 [2]

[a] Difference (%) between $\bar{E}_{s,ext}$ and $\bar{E}_{r,ext}$ was obtained using following expression $\frac{\bar{E}_{s,ret}-\bar{E}_{s,ext}}{\bar{E}_{s,avg}} \times 100$

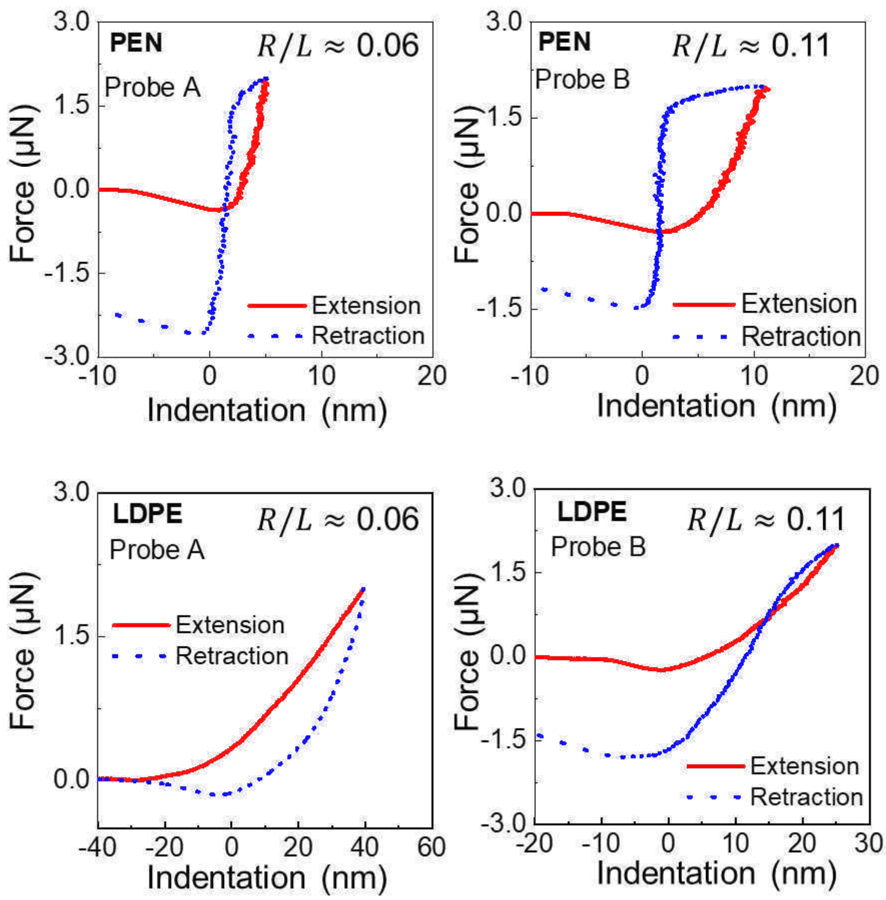

Figure 4.4 Typical force-indentation curves of PEN and LDPE specimens obtained by probes A and B

Contribution of R/L ratio on friction-induced hysteresis in force-indentation curves can be seen in comparison of force-indentation curves obtained on the same specimens using different probes. For example, force-indentation curve obtained on PEN specimen using probe A shows lower difference between extension and retraction curves than one obtained using probe B. In particular, retraction curves of force-indentation curves obtained on PEN specimen using probe B show infinite slopes, even negative due to large friction. It can be seen that larger relative size of colloidal tip leads to larger friction-induced hysteresis, and force-indentation curves obtained on PEN specimen using probe B were not interpreted. This suggests that relative size of colloidal tip should be reduced to minimize friction-induced hysteresis. However, small colloidal tip may lead to plastic deformation on relatively soft specimen, such as LDPE, as shown in Figure 4.4. Force-indentation curves obtained on the LDPE specimen using probe A exhibits plastic deformation whereas the one obtained by the probe B is dominated by elastic deformation. Contact pressure between LDPE specimen and probe A was estimated to be 5.4 MPa that exceed yield strength of LDPE polymers, typical ranged from 5 to 20 MPa. Force-indentation curves obtained on LDPE specimen using probe A were not interpreted. As for PMMA specimen, probe A was used to obtained force-indentation curves to reduce friction-induced hysteresis.

A major drawback of this work is that the proposed model only considering the effect of friction on the cantilever bending during AFM-based indentation measurements whereas the effect of friction on indentation of specimens was excluded since contact models considering sliding friction were likely not existing. Development of an adhesive contact model considering sliding friction needs to be investigated. In addition, friction forces in extension and retraction were also assumed to be equal in quantity and opposite in direction whereas the friction forces may be difference between different sliding direction [31]. A study of anisotropic of friction prior to AFM-based indentation measurements is also needed. Nevertheless, this work was expected to provide a better understanding of cantilever behavior during AFM-based indentation measurements, and thereby useful for accurate measurement of mechanical properties using an AFM.

5. CONCLUSIONS AND RECOMMENDATIONS

5.1 Conclusions

In this work, more evidences of friction-induced hysteresis were observed on force-indentation curves of the LDPE, PEN, and PMMA specimens, obtained by the colloidal tips. Friction-induced hysteresis as difference between extension and retraction curves were shown to be larger for the specimen have larger friction. In addition, a theoretical model was proposed for quantitatively determine elastic modulus and friction coefficient from force-indentation curves obtained from AFM-based indentation measurements. Elastic moduli and friction coefficients of the LDPE, PEN, PMMA specimens were determined using the proposed model to be 0.14 ± 0.05 GPa and 0.73 ± 0.32, 6.49 ± 2.40 and 1.29 ± 0.45, and, 4.07 ± 1.20 GPa and 0.87 ± 0.37, those were validated by elastic moduli of similar polymers taken from the literature and lateral force measurements, respectively. The proposed model was expected to be particularly helpful for investigation of in-situ relationship between friction properties and deformation in elastic contact from fundamental tribological point of view.

Furthermore, relative size of the colloidal tip to cantilever length were shown to contribute to friction-induced hysteresis in force-indentation curves. The colloidal tip plays a role as a torque for the friction force, and hence, it contributes to the friction-induced hysteresis. It was suggested that AFM probes with colloidal tips should be selected such that the R/L ratio is small to reduce effect of friction on force-indentation curves.

5.2 Recommendations for future works

Based on the limitations of this work, several recommendations were made for further investigation. Firstly, an adhesive contact model that considers friction should be investigated to quantify indentation of an adhesive specimen in presence of friction. Secondly, anisotropic friction properties of specimen should be investigated prior to the AFM-based indentation measurements, and hence, compensation of friction-induced hysteresis could be more precise. Finally, more data should be accumulated to identify the effect of friction during AFM-based indentation measurements.

REFERENCES

[1] E. A-Hassan, W.F. Heinz, M.D. Antonik, N.P. D'Costa, S. Nageswaran, C.-A. Schoenenberger, J.H. Hoh, Relative Microelastic Mapping of Living Cells by Atomic Force Microscopy, Biophysical Journal, 74 (1998) 1564-1578.

[2] C. Reynaud, F. Sommer, C. Quet, N. El Bounia, T.M. Duc, Quantitative determination of Young's modulus on a biphase polymer system using atomic force microscopy, Surface and Interface Analysis, 30 (2000) 185-189.

[3] B. Cappella, Mechanical Properties of Polymers Measured through AFM Force-Distance Curves, 2016.

[4] N.A. Burnham, R.J. Colton, H.M. Pollock, Interpretation issues in force microscopy, Journal of Vacuum Science & Technology A: Vacuum, Surfaces, and Films, 9 (1991) 2548-2556.

[5] H.-J. Butt, B. Cappella, M. Kappl, Force measurements with the atomic force microscope: Technique, interpretation and applications, Surface Science Reports, 59 (2005) 1-152.

[6] J.H. Hoh, A. Engel, Friction Effects on Force Measurements with an Atomic-Force Microscope, Langmuir, 9 (1993) 3310-3312.

[7] R.J. Warmack, X.Y. Zheng, T. Thundat, D.P. Allison, Friction Effects in the Deflection of Atomic-Force Microscope Cantilevers, Rev Sci Instrum, 65 (1994) 394-399.

[8] J. Stiernstedt, M.W. Rutland, P. Attard, A novel technique for the in situ calibration and measurement of friction with the atomic force microscope, Rev Sci Instrum, 76 (2005).

[9] J. Stiernstedt, M.W. Rutland, P. Attard, Erratum: "A novel technique for the in situ calibration and measurement of friction with the atomic force microscope" [Rev. Sci. Instrum. 76, 083710 (2005)], Rev Sci Instrum, 77 (2006).

[10] K. Chung, G.A. Shaw, J.R. Pratt, Accurate noncontact calibration of colloidal probe sensitivities in atomic force microscopy, Rev Sci Instrum, 80 (2009) 065107.

[11] J.R. Pratt, G.A. Shaw, L. Kumanchik, N.A. Burnham, Quantitative assessment of sample stiffness and sliding friction from force curves in atomic force microscopy, Journal of Applied Physics, 107 (2010).

[12] Q.D. Nguyen, K. Chung, Effect of Tip Shape on Nanomechanical Properties Measurements using AFM, Ultramicroscopy, (2019).

[13] Q.D. Nguyen, E.-S. Oh, K.-H. Chung, Nanomechanical properties of polymer binders for Li-ion batteries probed with colloidal probe atomic force microscopy, Polymer Testing, 76 (2019) 245-253.

[14] J.L. Hutter, Comment on tilt of atomic force microscope cantilevers: effect on spring constant and adhesion measurements, Langmuir, 21 (2005) 2630-2632.

[15] L.-O. Heim, M. Kappl, H.-J. Butt, Tilt of Atomic Force Microscope Cantilevers: Effect on Spring Constant and Adhesion Measurements, Langmuir, 20 (2004) 2760-2764.

[16] M.T. Hanson, T. Johnson, The Elastic Field for Spherical Hertzian Contact of Isotropic Bodies Revisited - Some Alternative Expressions, J Tribol-T Asme, 115 (1993) 327-332.

[17] A.R. Savkoor, G.A.D. Briggs, The Effect of Tangential Force on the Contact of Elastic Solids in Adhesion, Proceedings of the Royal Society A: Mathematical, Physical and Engineering Sciences, 356 (1977) 103-114.

[18] K.L. Johnson, K. Kendall, A.D. Roberts, Surface Energy and the Contact of Elastic Solids, Proceedings of the Royal Society A: Mathematical, Physical and Engineering Sciences, 324 (1971) 301-313.

[19] O. Pietrement, M. Troyon, General Equations Describing Elastic Indentation Depth and Normal Contact Stiffness versus Load, J Colloid Interface Sci, 226 (2000) 166-171.

[20] M. Rundlof, M. Karlsson, L. Wagberg, E. Poptoshev, M. Rutland, P. Claesson, Application of the JKR Method to the Measurement of Adhesion to Langmuir-Blodgett Cellulose Surfaces, J Colloid Interface Sci, 230 (2000) 441-447.

[21] A.-Y. Jee, M. Lee, Comparative analysis on the nanoindentation of polymers using atomic force microscopy, Polymer Testing, 29 (2010) 95-99.

[22] R. Suriano, C. Credi, M. Levi, S. Turri, AFM nanoscale indentation in air of polymeric and hybrid materials with highly different stiffness, Applied Surface Science, 311 (2014) 558-566.

[23] G.V. Samsonov, Mechanical Properties of the Elements, in: G.V. Samsonov (Ed.) Handbook of the Physicochemical Properties of the Elements, Springer US, Boston, MA, 1968, pp. 387-446.

[24] M.A. Lantz, S.J. O'Shea, A.C.F. Hoole, M.E. Welland, Lateral stiffness of the tip and tip-sample contact in frictional force microscopy, Applied Physics Letters, 70 (1997) 970-972.

[25] P. Attard, A. Carambassis, M.W. Rutland, Dynamic surface force measurement. 2. Friction and the atomic force microscope, Langmuir, 15 (1999) 553-563.

[26] J.L. Hutter, J. Bechhoefer, Calibration of atomic - force microscope tips, Rev Sci Instrum, 64 (1993) 1868-1873.

[27] R.G. Cain, S. Biggs, N.W. Page, Force Calibration in Lateral Force Microscopy, J Colloid Interface Sci, 227 (2000) 55-65.

[28] R.J. Cannara, M. Eglin, R.W. Carpick, Lateral force calibration in atomic force microscopy: A new lateral force calibration method and general guidelines for optimization, Rev Sci Instrum, 77 (2006).

[29] J.E. Sader, C.P. Green, In-plane deformation of cantilever plates with applications to lateral force microscopy, Rev Sci Instrum, 75 (2004) 878-883.

[30] K.-H. Chung, Y.-H. Lee, Y.-T. Kim, D.-E. Kim, J. Yoo, S. Hong, Nano-tribological characteristics of PZT thin film investigated by atomic force microscopy, Surface and Coatings Technology, 201 (2007) 7983-7991.

[31] A. Zmitrowicz, Models of kinematics dependent anisotropic and heterogeneous friction, International Journal of Solids and Structures, 43 (2006) 4407-4451.